Acta Mech 225, 2743–2760 (2014)
DOI 10.1007/s00707-014-1211-4

W. Q. Chen · B. Wu · C. L. Zhang · Ch. Zhang

On wave propagation in anisotropic elastic cylinders at nanoscale: surface elasticity and its effect

Received: 7 September 2013 / Revised: 6 December 2013 / Published online: 29 July 2014

Abstract Material heterogeneity induced by a surface or interface may be neglected at macroscale since the surface-to-volume ratio is usually small. However, its effect can become significant for structures at nanoscale with a large surface-to-volume ratio. In this paper, we incorporate such surface material heterogeneity into wave propagation analysis of a nanosized transversely isotropic cylinder. This is achieved by using the concept of surface elasticity. Instead of directly using the well-known Gurtin–Murdoch (GM) surface elasticity, we develop here another general framework based on a thin layer model. A novel approach based on state-space formalism is used to derive the approximate governing equations. Three different sources of surface effect can be identified in the first-order surface elasticity, i.e., the elasticity effect, the inertia effect and the thickness effect. It is found that the derived theory becomes identical to the GM surface elasticity if the thickness effect is dropped and when the material is isotropic. The axisymmetric wave propagation in a transversely isotropic cylinder with surface effect is then studied, and an exact solution is presented. Numerical results are finally given to show that the surface effect will play a very pronounced role in wave propagation in cylinders at nanoscale.

1 Introduction

Nanosized structures such as extremely thin films, nanobeams, nanotubes and nanowires have attracted much attention due to their applications in high-sensitive and high-frequency nanodevices such as MEMS/NEMS [1–3]. Understanding the mechanical behavior of these structures and devices is very important both in the design stage and in the application stage. In contrast to the macroscopic case, evidences from experiments and simulations have clearly indicated that the properties and responses of nanosized structures are mostly size-dependent [4–9]. One logical reasoning for this exotic characteristic is the surface effect, which accounts for the difference between the properties of a surface and its bulk. Physically, such material heterogeneity can be easily understood that atoms at or near a surface or interface usually sense different environments than their bulk counterparts [10–12].

Developing continuum mechanics models to account for the surface effect is very important since both experiment and numerical simulation down to the molecular and atomic levels are very expensive and

Presented at the Third Asian Conference on Mechanics of Functional Materials and Structures at the Indian Institute of Technology Delhi in New Delhi, India, December 5–8, 2012.

W. Q. Chen (✉) · B. Wu · C. L. Zhang
Soft Matter Research Center and Department of Engineering Mechanics, Zhejiang University, Hangzhou 310027, People's Republic of China
E-mail: chenwq@zju.edu.cn

Ch. Zhang
Department of Civil Engineering, University of Siegen, 57068 Siegen, Germany

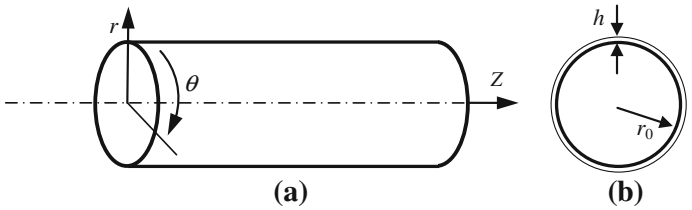

Fig. 1 **a** Solid cylinder and cylindrical coordinates, **b** cross section and thin surface material layer

time-consuming. A rigorous nonlinear framework of surface elasticity is already available, which was proposed by Gurtin and Murdoch [13] for a deformable material surface. We will refer to this theory as the GM theory, which can be seen as a generalization of the classical Young–Laplace equation [14] by taking the surface elasticity, in addition to the surface tension, into consideration. The GM theory has become very popular in recent years in the study of size-dependent properties and responses of nanosized materials and structures [15–21]. A further development of the GM theory can be found in Ref. [22], where a new energy functional was introduced to facilitate the derivation of all field equations at finite deformation.

The material surface in the GM theory has no thickness and is an idealization of the actual situation, which usually consists of several atomic layers. Historically and interestingly, Mindlin [23] derived the approximate governing equations for a very thin layer attached to a plate by following a systematic procedure for developing plate theories. It has been shown that Mindlin's equations will be identical to those in the GM theory when the residual surface tension is absent, provided the elastic properties are properly defined [24]. Later, Tiersten [25] investigated the elastic surface wave propagation in an elastic substrate guided by surface thin films using Mindlin's treatment to approximate the effect of thin films. We will refer to this treatment as the MT model later in this paper. The research along this line is also very fruitful. In particular, a different derivation technique based on the simple Taylor's series expansion has been proposed [26–30]. By this technique, the approximate governing equations of a surface or interface material layer of small thickness h can be obtained by truncating the series at an arbitrary order, say $O(h^n)$ with n being an integer. However, the derivation will become extremely tedious and tangly if more complexities (e.g., material anisotropy, multi-field coupling, etc.) are involved. Recently, a novel approach was suggested to overcome the difficulty by employing the state-space formalism [31,32].

In this paper, we will extend our previous works for plane boundary [31,32] to cylindrical boundary and explore the wave propagation behavior in a transversely isotropic elastic cylinder with surface effect. Waves in nanosized structures are a hot topic of current research [33–37]. Note that most available studies employ the GM theory to develop one-dimensional approximate rod or beam theories with surface effect for nanowires (or nanofibers or nanotubes) except the recent study by Huang and Kang [37], who presented an exact three-dimensional wave solution involving surface effect. None are concerned with material anisotropy. Here, we will pay our attention to: (i) deriving the governing equations of a material surface in cylindrical coordinates based on the MT model by virtue of the state-space formalism; (ii) obtaining the analytical solution of axisymmetric wave propagation in a transversely isotropic cylinder with surface effect; and (iii) numerically studying the thickness effect and anisotropy effect, both included in the developed surface elasticity theory, on the wave propagation behavior.

2 State-space formalism in cylindrical coordinates

Consider a transversely isotropic elastic solid cylinder with constant cross section. The material isotropic plane is perpendicular to the axis of the cylinder, which is taken to be identical to the z-axis of the cylindrical coordinate system (r, θ, z), see Fig. 1a.

The stress (σ_{ij})-displacement (u_i) constitutive relations for materials with transverse isotropy are [38]

$$\sigma_{rr} = c_{11}\frac{\partial u_r}{\partial r} + c_{12}\left(\frac{1}{r}\frac{\partial u_\theta}{\partial \theta} + \frac{u_r}{r}\right) + c_{13}\frac{\partial u_z}{\partial z},$$
$$\sigma_{\theta\theta} = c_{12}\frac{\partial u_r}{\partial r} + c_{11}\left(\frac{1}{r}\frac{\partial u_\theta}{\partial \theta} + \frac{u_r}{r}\right) + c_{13}\frac{\partial u_z}{\partial z},$$

$$\sigma_{zz} = c_{13}\frac{\partial u_r}{\partial r} + c_{13}\left(\frac{1}{r}\frac{\partial u_\theta}{\partial \theta} + \frac{u_r}{r}\right) + c_{33}\frac{\partial u_z}{\partial z},$$
$$\sigma_{rz} = c_{44}\left(\frac{\partial u_z}{\partial r} + \frac{\partial u_r}{\partial z}\right), \quad \sigma_{\theta z} = c_{44}\left(\frac{\partial u_\theta}{\partial z} + \frac{1}{r}\frac{\partial u_z}{\partial \theta}\right),$$
$$\sigma_{r\theta} = c_{66}\left(\frac{1}{r}\frac{\partial u_r}{\partial \theta} + \frac{\partial u_\theta}{\partial r} - \frac{u_\theta}{r}\right) \tag{1}$$

where $c_{66} = (c_{11} - c_{12})/2$ and c_{ij} are the elastic constants.

The equations of motion in cylindrical coordinates are

$$\begin{aligned}
\frac{\partial \sigma_{rr}}{\partial r} + \frac{1}{r}\frac{\partial \sigma_{r\theta}}{\partial \theta} + \frac{\partial \sigma_{rz}}{\partial z} + \frac{\sigma_{rr} - \sigma_{\theta\theta}}{r} &= \rho\frac{\partial^2 u_r}{\partial t^2},\\
\frac{\partial \sigma_{r\theta}}{\partial r} + \frac{1}{r}\frac{\partial \sigma_{\theta\theta}}{\partial \theta} + \frac{\partial \sigma_{\theta z}}{\partial z} + \frac{2\sigma_{r\theta}}{r} &= \rho\frac{\partial^2 u_\theta}{\partial t^2},\\
\frac{\partial \sigma_{rz}}{\partial r} + \frac{1}{r}\frac{\partial \sigma_{\theta z}}{\partial \theta} + \frac{\partial \sigma_{zz}}{\partial z} + \frac{\sigma_{rz}}{r} &= \rho\frac{\partial^2 u_z}{\partial t^2}
\end{aligned} \tag{2}$$

where ρ is the density, and t is the time variable.

In contrast to the conventional displacement method [39] which eliminates the six stress variables σ_{ij} from Eqs. (1) and (2) to obtain three coupled second-order partial differential equations about the three displacement components u_i, the state-space approach usually keeps three stress components and three displacement components and transforms the governing equations into a set of first-order ordinary differential equations with respect to one particular coordinate variable. The state-space approach has particular advantages over the displacement method in solving certain kinds of problems in mechanics and engineering, and the interested reader is referred to Refs. [38,40] for more details and references.

In this paper, we will derive the surface elasticity using the state-space formalism. In fact, from Eqs. (1) and (2), we can derive the following state equation [38]:

$$\frac{\partial \mathbf{Y}}{\partial r} = \mathbf{M}(c_{ij}, \rho;\ r;\ \partial_\theta,\ \partial_z,\ \partial_t)\mathbf{Y} \tag{3}$$

where $\mathbf{Y} = [u_r,\ u_\theta,\ u_z,\ \sigma_{rr},\ \sigma_{r\theta},\ \sigma_{rz}]^{\mathrm{T}}$ is the state vector (the superscript T signifies transpose), $\partial_\eta = \partial/\partial\eta$ $(\eta = \theta, z, t)$, and $\mathbf{M}$ is the 6×6 system matrix, with its four partitioned 3×3 sub-matrices being

$$\mathbf{M}_{11} = \begin{bmatrix} -\frac{c_{12}}{c_{11}}\frac{1}{r} & -\frac{c_{12}}{c_{11}}\frac{1}{r}\frac{\partial}{\partial\theta} & -\frac{c_{13}}{c_{11}}\frac{\partial}{\partial z} \\ -\frac{1}{r}\frac{\partial}{\partial\theta} & \frac{1}{r} & 0 \\ -\frac{\partial}{\partial z} & 0 & 0 \end{bmatrix}, \quad \mathbf{M}_{12} = \begin{bmatrix} \frac{1}{c_{11}} & 0 & 0 \\ 0 & \frac{1}{c_{66}} & 0 \\ 0 & 0 & \frac{1}{c_{44}} \end{bmatrix},$$

$$\mathbf{M}_{21} = \begin{bmatrix} \rho\frac{\partial^2}{\partial t^2} + \frac{a_1}{r^2} & \frac{a_1}{r^2}\frac{\partial}{\partial\theta} & \frac{a_2}{r}\frac{\partial}{\partial z} \\ -\frac{a_1}{r^2}\frac{\partial}{\partial\theta} & \rho\frac{\partial^2}{\partial t^2} - \frac{a_1}{r^2}\frac{\partial^2}{\partial\theta^2} - c_{44}\frac{\partial^2}{\partial z^2} & -\frac{(c_{44}+a_2)}{r}\frac{\partial^2}{\partial\theta\partial z} \\ -\frac{a_2}{r}\frac{\partial}{\partial z} & -\frac{(c_{44}+a_2)}{r}\frac{\partial^2}{\partial\theta\partial z} & \rho\frac{\partial^2}{\partial t^2} - \frac{c_{44}}{r^2}\frac{\partial^2}{\partial\theta^2} - a_3\frac{\partial^2}{\partial z^2} \end{bmatrix},$$

$$\mathbf{M}_{22} = \begin{bmatrix} \left(\frac{c_{12}}{c_{11}} - 1\right)\frac{1}{r} & -\frac{1}{r}\frac{\partial}{\partial\theta} & -\frac{\partial}{\partial z} \\ -\frac{c_{12}}{c_{11}}\frac{1}{r}\frac{\partial}{\partial\theta} & -\frac{2}{r} & 0 \\ -\frac{c_{13}}{c_{11}}\frac{\partial}{\partial z} & 0 & -\frac{1}{r} \end{bmatrix}$$

with $a_1 = c_{11} - c_{12}^2/c_{11}$, $a_2 = c_{13} - c_{12}c_{13}/c_{11}$ and $a_3 = c_{33} - c_{13}^2/c_{11}$.

In addition to the state equation in Eq. (3), a set of output equations is usually needed for the determination of other stress components. However, for our purpose in this paper, these are not necessary and hence are

omitted for simplicity. It is also noted here that the state equation in Eq. (3) for transversely isotropic materials can be easily generalized to the full anisotropy case [41], and even to cases when multi-field coupling is present [42].

3 Surface elasticity for a cylindrical material boundary

In this section, we will adopt the MT model to establish surface elasticity for a cylindrical material boundary. Thus, the cylindrical boundary is seen as a thin elastic cylindrical shell of thickness $h = r_1 - r_0$, with r_0 and r_1 being the inner and outer radii of the shell, respectively, see Fig. 1b. For clarity, a superscript s will be used in the following to indicate the quantities that are associated with the cylindrical shell.

Applying Eq. (3) to the cylindrical shell, we get

$$\frac{\partial \mathbf{Y}^s}{\partial r} = \mathbf{M}^s \left(c_{ij}^s, \rho^s; r; \partial_\theta, \partial_z, \partial_t \right) \mathbf{Y}^s \tag{4}$$

where $\mathbf{M}^s$ is the system matrix of the cylindrical shell, which contains three partial differential operators $\partial_\theta, \partial_z, \partial_t$. In addition, in contrast to the plane boundary [31,32], it depends obviously on the radial coordinate r. Thus, even if we treat the three partial differential operators as parameters [43], it is still difficult to write out the analytical solution (in the operator sense) to Eq. (4) in a simple form directly. Considering the fact that the material boundary layer is very thin (i.e., h is very small), we can make the approximation by taking $r \approx r_0$. Thus, we have

$$\frac{\partial \mathbf{Y}^s}{\partial r} = \mathbf{M}_0^s \left(c_{ij}^s, \rho^s; r_0; \partial_\theta, \partial_z, \partial_t \right) \mathbf{Y}^s \tag{5}$$

where $\mathbf{M}_0^s = \mathbf{M}^s|_{r=r_0}$. Now, all coefficients in Eq. (5) are constant and do not vary with the radial coordinate r.

Then, the solution to Eq. (5) can be formally written as

$$\mathbf{Y}^s(r) = \exp\left[\mathbf{M}_0^s (r - r_0)\right] \mathbf{Y}^s(r_0) \tag{6}$$

where, as mentioned earlier, the three partial differential operators $\partial_\theta, \partial_z, \partial_t$ have been seen as three usual parameters [31,43].

Setting $r = r_1$ in Eq. (6) leads to the following transfer relation between the state vectors at the outer and inner surfaces of the cylindrical shell:

$$\mathbf{Y}^s(r_1) = \mathbf{T}\mathbf{Y}^s(r_0) \tag{7}$$

where $\mathbf{T} = \exp(\mathbf{M}_0^s h)$ is the transfer matrix, a matrix exponential in the operator sense. By the definition of matrix exponential, we know that

$$\mathbf{T} = \mathbf{I} + \mathbf{M}_0^s h + \frac{1}{2}(\mathbf{M}_0^s)^2 h^2 + \cdots + \frac{1}{n!}(\mathbf{M}_0^s)^n h^n + O(h^{n+1}). \tag{8}$$

Thus, to the first order, we get from Eq. (7)

$$\mathbf{Y}^s(r_1) = (\mathbf{I} + \mathbf{M}_0^s h)\mathbf{Y}^s(r_0) + O(h^2) \approx (\mathbf{I} + \mathbf{M}_0^s h)\mathbf{Y}^s(r_0). \tag{9}$$

At the interface $r = r_0$, the state variables at the inner surface of the cylindrical shell should be equal to those of the bulk material, i.e.,

$$\mathbf{Y}^s(r_0) = \mathbf{Y}(r_0) \tag{10}$$

where $\mathbf{Y}$ (without the superscript s) denotes the state vector associated with the bulk material.

If the outer surface of the shell is free from tractions, we get from Eqs. (9) and (10)

$$\mathbf{M}_{021}^s h \left[u_r, u_\theta, u_z\right]^{\mathrm{T}} + \left[\sigma_{rr}, \sigma_{r\theta}, \sigma_{rz}\right]^{\mathrm{T}} + \mathbf{M}_{022}^s h \left[\sigma_{rr}, \sigma_{r\theta}, \sigma_{rz}\right]^{\mathrm{T}} = 0 \quad (r = r_0) \tag{11}$$

where $\mathbf{M}^s_{0ij}$ are the 3×3 partitioned sub-matrices of the system matrix $\mathbf{M}^s_0$. Thus, we have

$$\mathbf{M}^s_{021} = \begin{bmatrix} \rho^s \frac{\partial^2}{\partial t^2} + \frac{a^s_1}{r_0^2} & \frac{a^s_1}{r_0^2}\frac{\partial}{\partial\theta} & \frac{a^s_2}{r_0}\frac{\partial}{\partial z} \\ -\frac{a^s_1}{r_0^2}\frac{\partial}{\partial\theta} & \rho^s \frac{\partial^2}{\partial t^2} - \frac{a^s_1}{r_0^2}\frac{\partial^2}{\partial\theta^2} - c^s_{44}\frac{\partial^2}{\partial z^2} & -\frac{(c^s_{44}+a^s_2)}{r_0}\frac{\partial^2}{\partial\theta\partial z} \\ -\frac{a^s_2}{r_0}\frac{\partial}{\partial z} & -\frac{(c^s_{44}+a^s_2)}{r_0}\frac{\partial^2}{\partial\theta\partial z} & \rho^s \frac{\partial^2}{\partial t^2} - \frac{c^s_{44}}{r_0^2}\frac{\partial^2}{\partial\theta^2} - a^s_3\frac{\partial^2}{\partial z^2} \end{bmatrix},$$

$$\mathbf{M}^s_{022} = \begin{bmatrix} \left(\frac{c^s_{12}}{c^s_{11}} - 1\right)\frac{1}{r_0} & -\frac{1}{r_0}\frac{\partial}{\partial\theta} & -\frac{\partial}{\partial z} \\ -\frac{c^s_{12}}{c^s_{11}}\frac{1}{r_0}\frac{\partial}{\partial\theta} & -\frac{2}{r_0} & 0 \\ -\frac{c^s_{13}}{c^s_{11}}\frac{\partial}{\partial z} & 0 & -\frac{1}{r_0} \end{bmatrix} \tag{12}$$

with $a^s_1 = c^s_{11} - (c^s_{12})^2/c^s_{11}$, $a^s_2 = c^s_{13} - c^s_{12}c^s_{13}/c^s_{11}$, and $a^s_3 = c^s_{33} - (c^s_{13})^2/c^s_{11}$.

Equation (11) presents the governing equations of the first-order surface elasticity theory or the $O(h)$ effective boundary conditions for a cylindrical material surface which takes account of material transverse isotropy. We can identify three different sources of surface effect in this theory, i.e., the elasticity effect, the inertia effect and the thickness effect. The thickness effect corresponds to the last term in Eq. (11), the inertia effect corresponds to the second-order time-derivatives in the first term, while the rest in the first term is attributed to the elasticity of the material surface.

4 Comparison with the GM theory

The GM theory assumes zero-thickness of the material surface. If we neglect the thickness effect in Eq. (11), we have

$$\mathbf{M}^s_{021} h \left[u_r, u_\theta, u_z\right]^{\mathrm{T}} + \left[\sigma_{rr}, \sigma_{r\theta}, \sigma_{rz}\right]^{\mathrm{T}} = 0 \qquad (r = r_0). \tag{13}$$

Assuming the cylindrical shell is isotropic, we have

$$c^s_{11} = c^s_{33} = \lambda^s + 2\mu^s, \quad c^s_{12} = c^s_{13} = \lambda^s, \quad c^s_{44} = c^s_{66} = (c^s_{11} - c^s_{12})/2 = \mu^s \tag{14}$$

where λ^s and μ^s are the Lamé constants of the surface material. In view of Eqs. (12) and (14), we get from Eq. (13)

$$\begin{aligned} &\left(\rho^s h \frac{\partial^2}{\partial t^2} + \frac{a^s_1 h}{r_0^2}\right) u_r + \frac{a^s_1 h}{r_0^2}\frac{\partial u_\theta}{\partial\theta} + \frac{a^s_2 h}{r_0}\frac{\partial u_z}{\partial z} + \sigma_{rr} = 0, \\ &-\frac{a^s_1 h}{r_0^2}\frac{\partial u_r}{\partial\theta} + \left(\rho^s h \frac{\partial^2}{\partial t^2} - \frac{a^s_1 h}{r_0^2}\frac{\partial^2}{\partial\theta^2} - \mu^s h \frac{\partial^2}{\partial z^2}\right) u_\theta - \frac{a^s_4 h}{r_0}\frac{\partial^2 u_z}{\partial\theta\partial z} + \sigma_{r\theta} = 0, \\ &-\frac{a^s_2 h}{r_0}\frac{\partial u_r}{\partial z} - \frac{a^s_4 h}{r_0}\frac{\partial^2 u_\theta}{\partial\theta\partial z} + \left(\rho^s h \frac{\partial^2}{\partial t^2} - \frac{\mu^s h}{r_0^2}\frac{\partial^2}{\partial\theta^2} - a^s_3 h \frac{\partial^2}{\partial z^2}\right) u_z + \sigma_{rz} = 0 \end{aligned} \tag{15}$$

where

$$a^s_1 = a^s_3 = \frac{4\mu^s(\lambda^s + \mu^s)}{\lambda^s + 2\mu^s}, \quad a^s_2 = \frac{2\mu^s\lambda^s}{\lambda^s + 2\mu^s}, \quad a^s_4 = \mu^s + a^s_2 = \frac{\mu^s(3\lambda^s + 2\mu^s)}{\lambda^s + 2\mu^s}. \tag{16}$$

By defining the following surface material constants:

$$\rho_0 = \rho^s h, \quad \mu_0 = \mu^s h, \quad \lambda_0 = 2\mu^s\lambda^s h/\left(\lambda^s + 2\mu^s\right), \tag{17}$$

we have

$$\lambda_0 + \mu_0 = \frac{\mu^s(3\lambda^s + 2\mu^s)}{\lambda^s + 2\mu^s} h, \quad \lambda_0 + 2\mu_0 = \frac{4\mu^s(\lambda^s + \mu^s)}{\lambda^s + 2\mu^s} h. \tag{18}$$

Then, Eq. (15) can be rewritten as

$$\begin{aligned}
&\left(\rho_0\frac{\partial^2}{\partial t^2}+\frac{\lambda_0+2\mu_0}{r_0^2}\right)u_r+\frac{\lambda_0+2\mu_0}{r_0^2}\frac{\partial u_\theta}{\partial\theta}+\frac{\lambda_0}{r_0}\frac{\partial u_z}{\partial z}+\sigma_{rr}=0,\\
&-\frac{\lambda_0+2\mu_0}{r_0^2}\frac{\partial u_r}{\partial\theta}+\left(\rho_0\frac{\partial^2}{\partial t^2}-\frac{\lambda_0+2\mu_0}{r_0^2}\frac{\partial^2}{\partial\theta^2}-\mu_0\frac{\partial^2}{\partial z^2}\right)u_\theta-\frac{\lambda_0+\mu_0}{r_0}\frac{\partial^2 u_z}{\partial\theta\partial z}+\sigma_{r\theta}=0,\\
&-\frac{\lambda_0}{r_0}\frac{\partial u_r}{\partial z}-\frac{\lambda_0+\mu_0}{r_0}\frac{\partial^2 u_\theta}{\partial\theta\partial z}+\left[\rho_0\frac{\partial^2}{\partial t^2}-\frac{\mu_0}{r_0^2}\frac{\partial^2}{\partial\theta^2}-(\lambda_0+2\mu_0)\frac{\partial^2}{\partial z^2}\right]u_z+\sigma_{rz}=0.
\end{aligned}\tag{19}$$

It is easily found that Eq. (19) is the same as Eq. (A8) in "Appendix 1", which corresponds to the GM surface elasticity when the surface tension is absent. Thus, we can conclude that the MT model, along with the proposed efficient derivation using the state-space formalism, can lead to the same equations as the GM theory, provided that the thickness effect in the first-order approximation is omitted and the surface material properties are properly defined. Interestingly, as seen from Eq. (17), the surface material constants ρ_0 and μ_0 are merely the scaled versions of their bulk counterparts, while λ_0 is more involved. This fact has also been noticed by Gurtin and Murdoch for a plane material surface [24].

5 Axisymmetric waves in cylinders with surface effect

5.1 Axisymmetric wave solution

Consider linear elastic waves propagating in an infinitely long transversely isotropic cylinder. For illustration purpose, we consider only axisymmetric torsionless waves in which the motion is independent of the circumferential coordinate θ and $u_\theta = 0$. The harmonic traveling wave solution may be sought in the following form:

$$\begin{aligned}
u_r &= U_r(r)\sin(kz-\omega t),\\
u_z &= U_z(r)\cos(kz-\omega t)
\end{aligned}\tag{20}$$

where k denotes the axial wave number, ω the circular frequency, and $U_r(r)$ and $U_z(r)$ the unknown mode distribution functions along the radial direction. Substituting Eq. (20) into Eq. (1) yields the following stress components:

$$\begin{aligned}
&\sigma_{rr}\equiv T_{rr}\sin(kz-\omega t),\quad \sigma_{\theta\theta}\equiv T_{\theta\theta}\sin(kz-\omega t),\quad \sigma_{zz}\equiv T_{zz}\sin(kz-\omega t),\\
&\sigma_{rz}\equiv T_{rz}\cos(kz-\omega t),\quad \sigma_{\theta z}=\sigma_{r\theta}=0
\end{aligned}\tag{21}$$

where

$$\begin{aligned}
&T_{rr}=c_{11}\frac{\partial U_r}{\partial r}+c_{12}\frac{U_r}{r}-c_{13}kU_z,\quad T_{\theta\theta}=c_{12}\frac{\partial U_r}{\partial r}+c_{11}\frac{U_r}{r}-c_{13}kU_z,\\
&T_{zz}=c_{13}\frac{\partial U_r}{\partial r}+c_{13}\frac{U_r}{r}-c_{33}kU_z,\quad T_{rz}=c_{44}\left(\frac{\partial U_z}{\partial r}+kU_r\right).
\end{aligned}\tag{22}$$

By substituting Eq. (21) into Eq. (2), we obtain

$$\begin{aligned}
&c_{11}\frac{\partial^2 U_r}{\partial r^2}+\frac{c_{11}}{r}\frac{\partial U_r}{\partial r}-c_{11}\frac{U_r}{r^2}-c_{44}k^2U_r-c_{13}k\frac{\partial U_z}{\partial r}-c_{44}k\frac{\partial U_z}{\partial r}=-\rho\omega^2U_r,\\
&k\left(c_{44}\frac{\partial U_r}{\partial r}+c_{13}\frac{\partial U_r}{\partial r}+c_{13}\frac{U_r}{r}+\frac{c_{44}}{r}U_r\right)-k^2c_{33}U_z+\frac{c_{44}}{r}\frac{\partial U_z}{\partial r}\\
&+c_{44}\frac{\partial^2 U_z}{\partial r^2}=-\rho\omega^2U_z.
\end{aligned}\tag{23}$$

The solution to Eq. (23) takes the following form:

$$U_r=AJ_1(\alpha r),\quad U_z=BJ_0(\alpha r)\tag{24}$$

where A and B are constants to be determined, $J_n(\cdot)$ is the Bessel function of first kind and n-th order, and α is the wave number in the radial direction. Upon substituting Eq. (24) into Eq. (23), we find

$$\begin{aligned}(\rho\omega^2 - c_{11}\alpha^2 - c_{44}k^2)A + (c_{13}+c_{44})k\alpha B = 0,\\ (c_{13}+c_{44})k\alpha A + \left(\rho\omega^2 - c_{44}\alpha^2 - c_{33}k^2\right)B = 0.\end{aligned} \tag{25}$$

The compatibility of Eq. (25) requires that

$$\begin{vmatrix} \rho\omega^2 - c_{11}\alpha^2 - c_{44}k^2 & (c_{13}+c_{44})k\alpha \\ (c_{13}+c_{44})k\alpha & \rho\omega^2 - c_{44}\alpha^2 - c_{33}k^2 \end{vmatrix} = 0 \tag{26}$$

which results in a characteristic equation. It is a quadratic algebraic equation of α^2, from which we can obtain four roots of α. Without loss of generality, we assume $\mathrm{Re}[\alpha_i] > 0$ or $\mathrm{Re}[\alpha_i] = 0$ and $\mathrm{Im}[\alpha_i] > 0$ $(i = 1, 2)$. It is noted that if the first-kind Bessel functions in Eq. (24) are replaced with the second-kind ones, the solution still satisfies Eq. (23), but it becomes unbounded at $r = 0$ and hence is omitted here.

Therefore, the complete wave solution to Eq. (23) can be written as

$$U_r(r) = \sum_{i=1}^{2} A_i J_1(\alpha_i r), \quad U_z(r) = \sum_{i=1}^{2} p_i A_i J_0(\alpha_i r) \tag{27}$$

where A_i $(i = 1, 2)$ are undetermined constants, p_i $(i = 1, 2)$ are the modal ratios that can be determined from any one of the following two equations:

$$\begin{aligned}(\rho\omega^2 - c_{11}\alpha_i^2 - c_{44}k^2) + (c_{13}+c_{44})\,k\alpha_i\, p_i = 0,\\ (c_{13}+c_{44})k\alpha_i + \left(\rho\omega^2 - c_{44}\alpha_i^2 - c_{33}k^2\right)p_i = 0.\end{aligned} \tag{28}$$

5.2 Dispersion relation

In the following, we use Eq. (13) instead of Eq. (11) to derive the wave dispersion equation for cylinders with surface effect. This is because the associated formulae become simpler, while the integrality of derivation remains the same as that when the thickness effect is involved. For axisymmetric waves, Eq. (13) becomes

$$\begin{aligned}\left(\rho^s h\frac{\partial^2}{\partial t^2} + \frac{a_1^s h}{r_0^2}\right)u_r + \frac{a_2^s h}{r_0}\frac{\partial u_z}{\partial z} + \sigma_{rr} = 0,\\ -\frac{a_2^s h}{r_0}\frac{\partial u_r}{\partial z} + \left(\rho^s h\frac{\partial^2}{\partial t^2} - a_3^s h\frac{\partial^2}{\partial z^2}\right)u_z + \sigma_{rz} = 0\end{aligned} \tag{29}$$

which can be seen as the effective boundary conditions at the cylindrical surface $r = r_0$. Making use of the wave solution presented above, we obtain from Eq. (29)

$$\sum_{i=1}^{2} f_{ji} A_i = 0 \qquad (j = 1, 2) \tag{30}$$

where

$$\begin{aligned}f_{1i} &= \left(-\rho^s h\omega^2 + \frac{a_1^s h}{r_0^2} - \frac{2c_{66}}{r_0}\right)J_1(\alpha_i r_0) + \left(c_{11}\alpha_i - c_{13}kp_i - \frac{a_2^s hk}{r_0}\right)p_i J_0(\alpha_i r_0),\\ f_{2i} &= (-\rho^s\omega^2 + a_3^s k^2)p_i h J_0(\alpha_i r_0) + \left[c_{44}(k - \alpha_i p_i) - \frac{a_2^s hk}{r_0}\right]J_1(\alpha_i r_0).\end{aligned} \tag{31}$$

Equation (30) is a set of two linear homogeneous algebraic equations about A_i $(i = 1, 2)$. For nontrivial solutions, we get

$$f_{11}f_{22} - f_{12}f_{21} = 0 \tag{32}$$

which gives the dispersion relation for axisymmetric torsionless waves in a cylinder with surface effect.

Again, we emphasize here that the characteristic dispersion equation in the case that the thickness effect is kept can be similarly derived, and the final result is given in "Appendix 2". We shall study the thickness effect numerically in the following section.

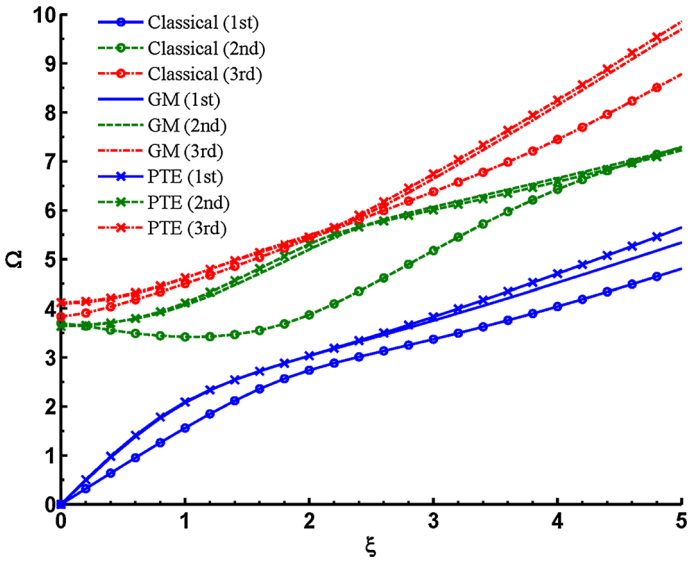

Fig. 2 Axisymmetric wave dispersion curves for an isotropic iron cylinder ($r_h = 0.1,\ r_\rho = 0.5,\ r_c = 8$)

6 Numerical results and discussion

In this section, we will conduct numerical simulations of axisymmetric wave propagation in elastic cylinders of different sizes by adopting the proposed surface elasticity theory to study the surface effect on wave characteristics. An isotropic crystal cylinder made of iron is first considered to investigate the thickness effect, which is not included in the GM theory. Then, two anisotropic materials, i.e., the cubic and hexagonal crystals, are chosen to show the effect of material anisotropy on the wave propagation behavior. We shall use the dimensionless frequency and wave number defined by $\Omega = r_0\omega\sqrt{\rho/c_{44}}$ and $\xi = kr_0$, respectively, in the following discussion.

On one hand, there are very few accurate data available in the literature regarding surface elastic properties. Those calculated from molecular dynamics are more qualitative than quantitative. On the other hand, our model clearly reveals the physical nature of these properties, as already noticed by Gurtin and Murdoch [24]. Thus, it is more direct and convenient to assign the bulk material constants (with superscript s) to the surface layer. In addition, we will adopt the following dimensionless quantities:

$$r_\rho = \rho^s/\rho,\ \ r_c = c^s_{ij}/c_{ij},\ \ r_h = h/r_0 \tag{33}$$

to study the surface effect for different surface properties.

For simplicity, three abbreviations, namely classical, GM and PTE, will be used below, which denote the classical elasticity without surface effect, the GM surface theory without thickness effect and the present surface theory with thickness effect, respectively.

6.1 Thickness effect

The material constants of iron are taken to be: $\lambda = 80\,\text{GPa},\ \mu = 70\,\text{GPa}$ and $\rho = 7{,}000\,\text{kg/m}^3$ [24]. The lowest three branches of the axisymmetric wave dispersion relations are depicted in Fig. 2 for $r_h = 0.1$, $r_\rho = 0.5$ and $r_c = 8$. These three branches generally correspond to the extensional (longitudinal), radial and axial-shear motions, respectively, at least dominating at a low wave number [44]. The results from three different theories (i.e., classical, GM, and PTE) are all compared in the figure. It is found that, while the predictions from GM and PTE agree quite well for this example, the surface effect plays an important role in the wave propagation even at a relatively low wave number.

The nonzero cutoff frequencies at $k = 0$ can be determined analytically from the dispersion equation, as shown in "Appendix 2" for PTE. The results for classical and GM can be obtained by a simple degenerate analysis. It is noted that the two cutoff frequencies, corresponding to the first radial mode ($\Omega_r^{(1)}$) and the first

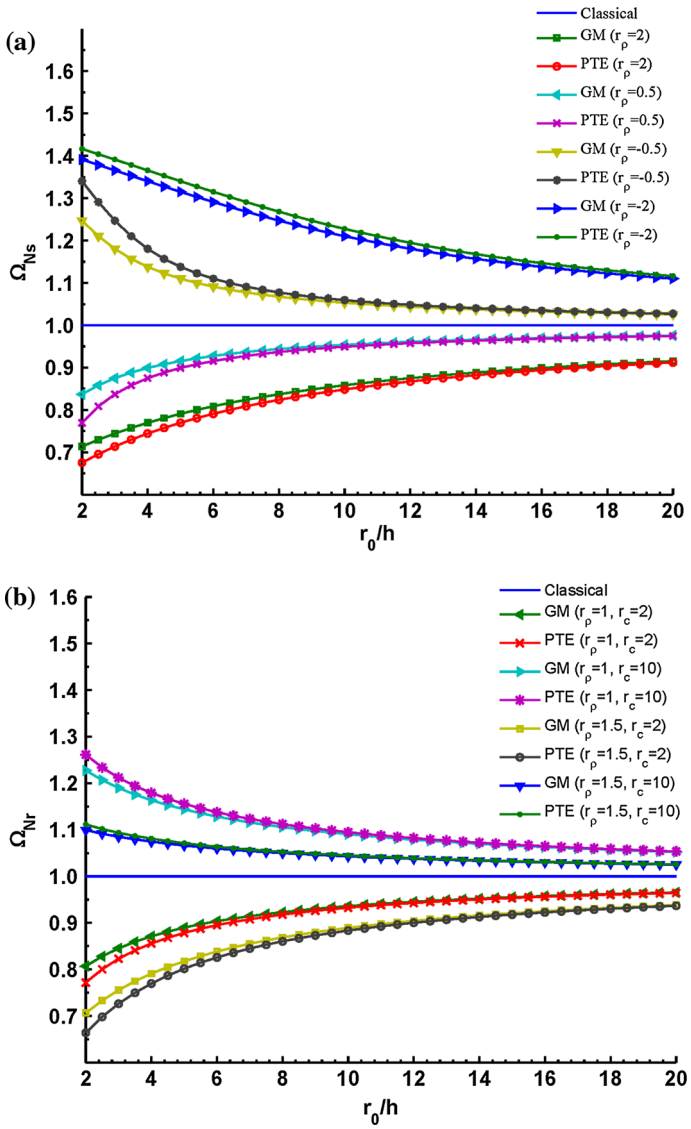

Fig. 3 Normalized cutoff frequency versus r_0/h for different surface parameters for **a** axial-shear mode, and **b** radial mode

axial-shear mode ($\Omega_s^{(1)}$), can be clearly identified. Interestingly, when no surface effect is involved, the cutoff frequency for the first radial mode ($\Omega_r^{(1)}$) is lower than that for the first axial-shear mode ($\Omega_s^{(1)}$), but if the surface effect is included, $\Omega_r^{(1)}$ becomes larger than $\Omega_s^{(1)}$. According to Eq. (B3), $\Omega_s^{(1)}$ is independent of r_c, and once r_h and r_ρ are given, $\Omega_s^{(1)}$ will keep unchanged. On the other hand, $\Omega_r^{(1)}$ depends on r_c, and hence, when the material parameters are properly chosen, the relative magnitude between $\Omega_s^{(1)}$ and $\Omega_r^{(1)}$ can be switched.

In order to clearly show the thickness effect on the wave propagation behavior, the curves of normalized cutoff frequencies Ω_{Ns} and Ω_{Nr} (for the axial-shear mode and radial mode, respectively) versus r_0/h are shown in Fig. 3a, b for different combinations of r_ρ and r_c. The normalization is made with respect to the classical ones. Since $\Omega_s^{(1)}$ is independent of r_c, only r_ρ is varied to modulate the thickness effect as shown in Fig. 3a, while different combinations of r_c and r_ρ are considered in the calculation of Ω_{Nr} as shown in Fig. 3b. It is seen that both Ω_{Ns} and Ω_{Nr} approach 1 when r_0/h becomes infinitely large. This is expected since the surface effect becomes trivial at macroscale. It is also seen that the inclusion of the thickness effect in PTE will generally make the deviation from classical results more obvious than GM. This can be clearly seen from Fig. 3, especially for $r_0/h < 5$.

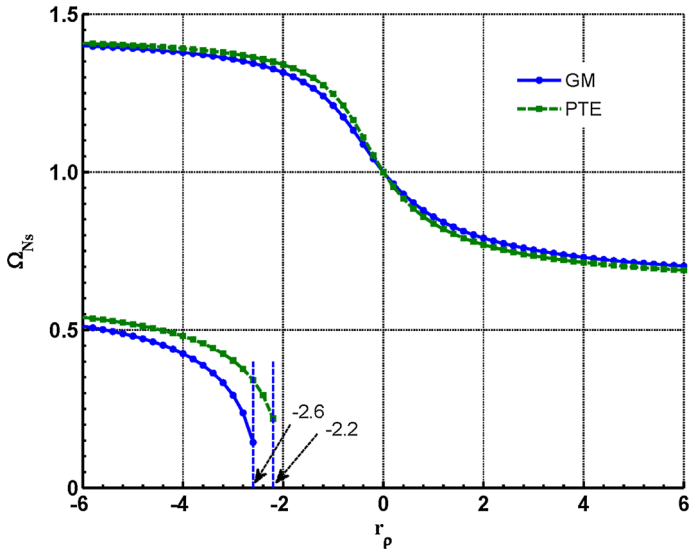

Fig. 4 Normalized cutoff frequency Ω_{Ns} versus $r_\rho (r_h = 0.1)$

Figure 3a also indicates that, for positive r_ρ, the surface effect lowers the cutoff frequency of the first axial-shear mode, while for negative r_ρ, the situation reverses accordingly. Note that the negative surface mass density was considered and discussed by Huang and Kang [37]; there are certain practical cases where negative macroscopic mass may be encountered [45]. The surface effect on the cutoff frequency of the first radial mode is more complicated, because it depends on both r_c and r_ρ. Figure 3b shows that, for positive r_ρ, $\Omega_r^{(1)}$ increases with r_c, but decreases with r_ρ. In fact, the larger the surface elastic constants, the stiffer the surface layer and the higher the natural frequency. On the contrary, the larger the positive surface mass density, the lower the frequency. It is thus clear that the surface effect on the cutoff frequencies can be quite different if different surface properties are involved.

The curves of the normalized cutoff frequency Ω_{Ns} for the axial-shear mode versus r_ρ are shown in Fig. 4 for $r_h = 0.1$. Both GM and PTE results are given. As is anticipated, $\Omega_{Ns} = 1$ when $r_\rho = 0$. It is seen that, due to the presence of surface effect, for positive r_ρ, $\Omega_s^{(1)}$ decreases with r_ρ, and $\Omega_s^{(1)}$ of PTE is lower than that of GM. However, for negative r_ρ, the situation changes. What's more, when r_ρ decreases approximately to a certain value (-2.2 and -2.6 for GM and PTE, respectively), a new branch will emerge with the cutoff frequency even lower than the continuous extension on the negative r_ρ side of the first axial-shear mode for positive r_ρ.

6.2 Anisotropy effect

It is interesting and also important to study the material anisotropy effect since quite a lot of materials exhibit strong anisotropy at nanoscale. Here, we take cubic crystals and hexagonal crystals as examples. For cubic crystals, we have three independent elastic constants and can define the following anisotropy ratio [46]:

$$A = \frac{2c_{44}}{c_{11} - c_{12}}. \tag{34}$$

Clearly, $A = 1$ corresponds to an isotropic material, and the degree of anisotropy is measured by the deviation of A from 1. In the numerical calculation, we assume $c_{11} = \lambda + 2\mu$ and $c_{12} = \lambda$ and calculate c_{44} by $c_{44} = A(c_{11} - c_{12})/2$ for the cubic crystals. We will take $\lambda = 52.4$ and $\mu = 68.1$ GPa, the Voigt average elastic constants for the cubic crystal Si [46].

For hexagonal crystals, we have five independent elastic constants. In accordance with Eq. (34), we may define the following three anisotropy ratios:

$$A_1 = \frac{2c_{44}}{c_{11} - c_{12}}, \quad A_2 = \frac{2c_{44}}{c_{11} - c_{13}}, \quad A_3 = \frac{2c_{44}}{c_{33} - c_{13}}. \tag{35}$$

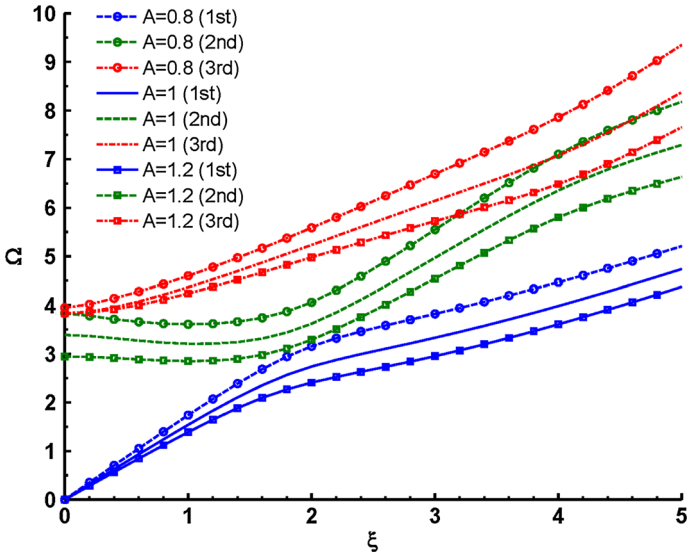

Fig. 5 Axisymmetric wave dispersion curves for cubic crystal cylinders ($r_h = 0.01,\ r_\rho = r_c = 1$)

When $A_1 = A_2 = A_3 = 1$, we have an isotropic material. In the numerical calculation, we assume $c_{11} = \lambda + 2\mu$ and $c_{12} = \lambda$, and calculate the other three constants for the hexagonal crystals according to

$$c_{44} = (c_{11} - c_{12})A_1/2, \quad c_{13} = c_{11} - 2c_{44}/A_2, \quad c_{33} = c_{13} + 2c_{44}/A_3. \tag{36}$$

We will take $E = 113.8\,\text{GPa}$ and $\nu = 0.357$, which are the averaged bulk Young's modulus and Poisson's ratio for the hexagonal crystal ZnO predicted by the first-principles DFT method [47]. Note that the two Lamé constants can be calculated from Young's modulus and Poisson's ratio via $\lambda = \nu E/[(1+\nu)(1-2\nu)]$ and $\mu = E/[2(1+\nu)]$.

The first three lowest branches of the axisymmetric wave dispersion curves for cubic crystal cylinders are given in Fig. 5 for $r_h = 0.01$ and $r_\rho = r_c = 1$. Different anisotropy ratios have been assumed, and the results are obtained with PTE. It is seen that the material anisotropy of the bulk and the surface has a significant influence on the wave propagation behavior, except the cutoff frequency $\Omega_s^{(1)}$, which is independent of A. In particular, we notice that $\Omega_s^{(1)}$ is higher than $\Omega_r^{(1)}$ when $A = 1$ (i.e., the material is isotropic), but when $A = 0.8$, $\Omega_s^{(1)}$ becomes lower than $\Omega_r^{(1)}$. Therefore, if an anisotropy effect is involved, the relative magnitude between these two cutoff frequencies may be changed.

Unlike Ω_s, Ω_r varies with the anisotropy ratio, which is shown in Fig. 6 for $r_h = 0.1$ and $r_\rho = r_c = 1$. All three results (classical, GM and PTE) are presented and compared in the figure. The GM and PTE results agree well and are lower than the classical ones. Generally, Ω_r changes rapidly when A deviates from 1 (i.e., the isotropic case), indicating a strong effect of material anisotropy. It is also of interest to note that when A reaches about 2.5, the curve of the originally first radial mode stops, while the curve of the originally second radial mode continues and turns to be the first radial mode, as long as a real frequency only is considered.

The curves of the cutoff frequency for the radial mode, $\Omega_r^{(1)}$, versus r_0/h are shown in Fig. 7 for $r_\rho = r_c = 1$ and different anisotropy ratios. Just like Fig. 2, the surface effect is significant when the radius of the cylinder is small, and both the GM and PTE predictions approach the classical ones when r_0 becomes infinitely large. It is noted that the classical predictions are affected by the material anisotropy, as clearly seen from Fig. 7.

The first three lowest branches of the axisymmetric wave dispersion curves for hexagonal crystal cylinders are given in Fig. 8 for $r_h = 0.01$, $r_\rho = 1$ and $r_c = 1$. Different combinations of the three anisotropy ratios are considered. The results are calculated using PTE. Just as the cubic cylinder, material anisotropy has an obvious effect on the dispersion curves. The cutoff frequencies of the axial-shear mode again keep unchanged when the three anisotropy ratios take different values. It is also observed that the curves for $A_1 = 1$, $A_2 = 0.8$ and $A_3 = 1.2$ are closest to the isotropic ones ($A_1 = A_2 = A_3 = 1$), indicating that the frequency is more sensitive to the anisotropy ratio A_1 than the other two anisotropy ratios A_2 and A_3.

It can be shown from "Appendix 2" that Ω_r depends on the anisotropy ratio A_1 only. This dependence is depicted in Fig. 9 for the cutoff frequency of the first radial mode $\Omega_r^{(1)}$ for $r_h = 0.1$ and $r_\rho = r_c = 1$. To

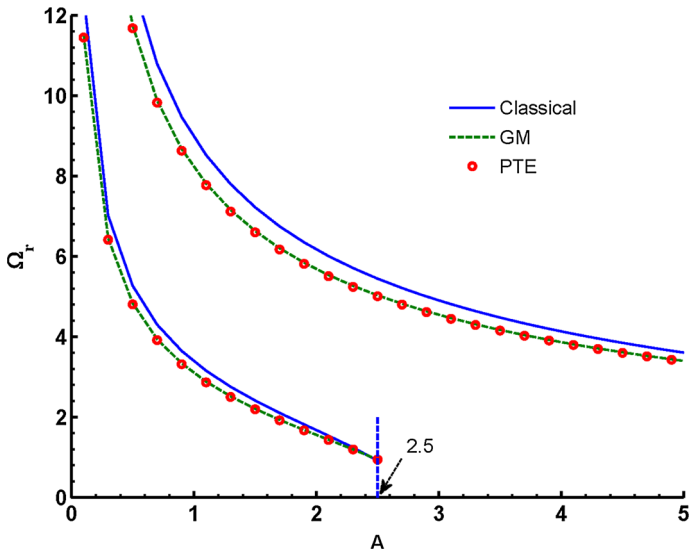

Fig. 6 Cutoff frequency Ω_r versus anisotropy ratio A ($r_h = 0.1$ and $r_\rho = r_c = 1$)

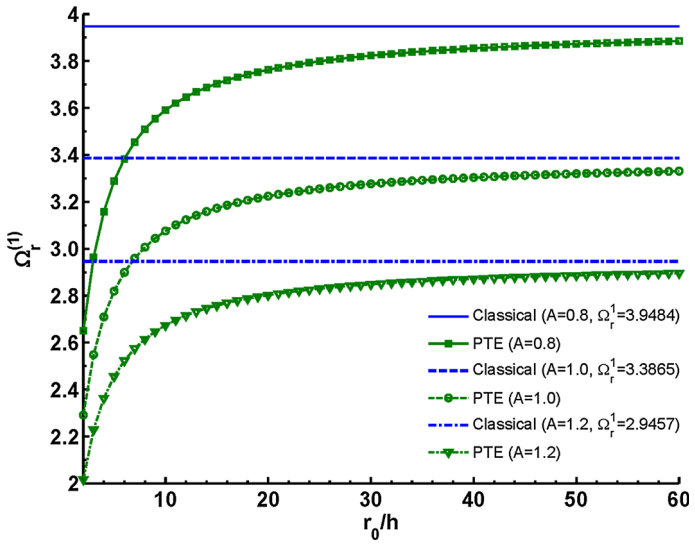

Fig. 7 Cutoff frequency versus r_0/h for different anisotropy ratios ($r_\rho = r_c = 1$)

ensure the positive definiteness of the elastic constant matrix, the anisotropy ratio A_1 must satisfy $0.2657 < A_1 < 4.2308$ for $A_2 = A_3 = 1$. The results of GM and PTE are almost the same, both deviating from the classical ones to a certain degree.

To check the accuracy of the proposed surface elasticity theory for anisotropic materials, we finally make a numerical comparison with the exact solution, which is obtained by treating the cylinder as a composite core-shell structure, with both the core and the shell modeled directly with the exact three-dimensional elasticity theory [38]. The material is hexagonal crystal ZnO, for which the material properties can be found in Ref. [38]. We take $r_h = 0.2$, $r_\rho = 2$ and $r_c = 5$. Figure 10 compares the first three lowest branches for the axisymmetric wave dispersion curves among GM, PTE and the exact solution. It is seen that PTE is closer to the exact theory than GM, indicating that the thickness effect may be important in certain situations involving material anisotropy.

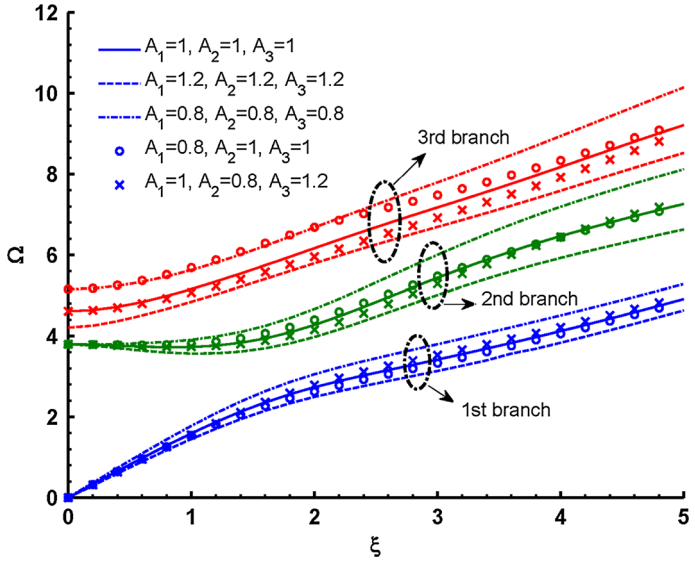

Fig. 8 Axisymmetric wave dispersion curves for hexagonal crystal cylinders ($r_h = 0.01,\ r_\rho = r_c = 1$)

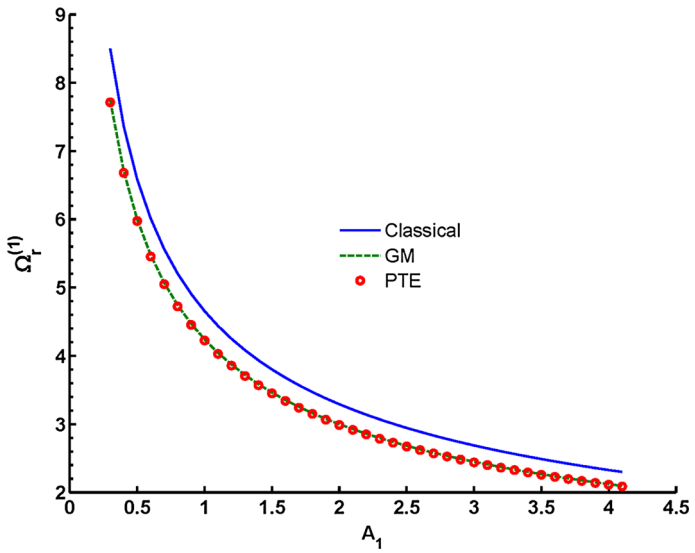

Fig. 9 Cutoff frequency $\Omega_r^{(1)}$ versus anisotropy ratio $A_1 (r_h = 0.1,\ r_\rho = r_c = 1)$

7 Conclusions

In this study, the surface elasticity theory for a cylindrical material boundary is established, which can account for material anisotropy. In contrast to the GM surface theory which assumes zero-thickness of the surface, we here treat the cylindrical surface as a thin cylindrical shell with very small thickness. This is known as the MT model proposed by Mindlin and Tiersten. A simple and convenient method is employed to derive the governing equations of the surface elasticity based on the state-space formalism. The obtained first-order approximate surface elasticity theory or the $O(h)$ effective boundary conditions includes three different contributions, corresponding to the elasticity effect, the inertia effect and the thickness effect, respectively. When the thickness effect is neglected, we obtain the same governing equations as the GM surface elasticity for isotropic materials and in absence of surface tension.

Numerical examples are particularly designed to show the thickness effect, which is omitted in the GM surface elasticity, and the material anisotropy effect, which has not been fully explored in wave analysis of

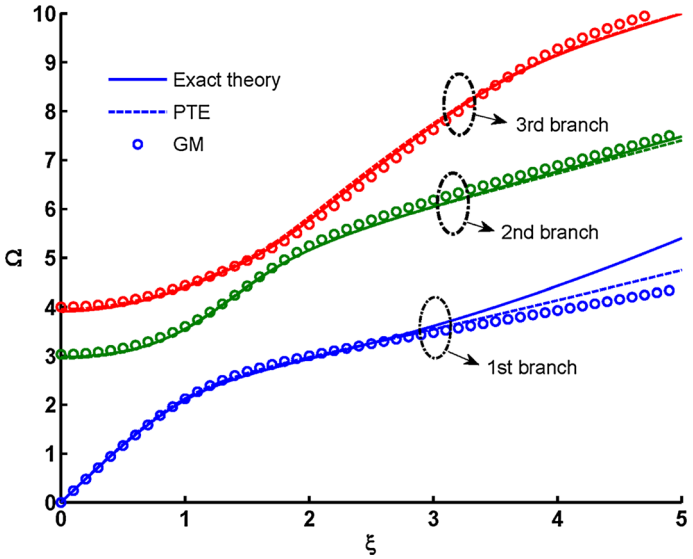

Fig. 10 Axisymmetric wave dispersion curves for a hexagonal crystal cylinder ($r_h = 0.2$, $r_\rho = 2$ and $r_c = 5$)

nanosized structures. The results have shown that both effects may become significant. Therefore, it is possible to modulate the waves in the cylinder (and other structures as well) by surface engineering.

It is strengthened that our method clearly indicates the physical nature of the surface material properties defined in the GM theory. Furthermore, this method is very convenient to be used in multi-field coupling cases even at finite deformation. It can also be adopted to develop accurate interface elasticity theories.

Finally, we would like to point out that the theory of surface elasticity is only one possible candidate, within the framework of (generalized) continuum mechanics, for interpreting various size-dependent phenomena associated with nanosized structures. Other generalized continuum mechanics theories, including the nonlocal elasticity theory and gradient elasticity theory in particular, have also been widely employed in the literature to study the size effects in the mechanical behavior of these very tiny structures [33,49–52]. A validation study and a comprehensive comparison among these theories should be very interesting from both theoretical and practical points of view, which however is beyond the scope of this study.

Acknowledgments The work was supported by the National Natural Science Foundation of China (Nos. 11090333, 11272281, and 11321202), the German Research Foundation (DFG, Project-No: ZH 15/20-1), and the joint project funded by the China Scholarship Council (CSC) and the German Academic Exchange Service (DAAD, Project-ID: 54392540).

Appendix 1: Equations for Gurtin–Murdoch surface elasticity in cylindrical coordinates

In tensor form, the geometric, constitutive and equilibrium equations in the GM surface elasticity for isotropic elastic materials are respectively:

$$\mathbf{E} = \left(\mathbf{D}_S\mathbf{u} + \mathbf{D}_S^{\mathrm{T}}\mathbf{u}\right)/2, \tag{A1.1}$$

$$\mathbf{\Sigma} = \tau_0\mathbf{I} + 2(\mu_0 - \tau_0)\mathrm{E} + (\lambda_0 + \tau_0)(tr\mathbf{E})\mathbf{I} + \tau_0(\mathrm{grad}_S\mathbf{u}), \tag{A1.2}$$

$$\mathrm{div}_S\mathbf{\Sigma} = \boldsymbol{\sigma}\,\mathbf{n} + \rho_0\ddot{\mathbf{u}} \tag{A1.3}$$

where ρ_0, λ_0 and μ_0 are the surface mass density and the surface Lamé constants, respectively; $\mathbf{\Sigma}$ and $\mathbf{E}$ denote the surface stress and surface strain fields; τ_0 is the residual surface tension; $\mathbf{n}$ the outward unit normal to the surface; and $\mathbf{I}$, tr, grad_S, div_S and $\mathbf{D}_S$ are all operators that are well defined in Ref. [13].

The displacement vector in cylindrical coordinates (r, θ, z) can be written as:

$$\mathbf{u} = u_r\mathbf{e}_r + u_\theta\mathbf{e}_\theta + u_z\mathbf{e}_z \tag{A2}$$

with $\mathbf{e}_i$ being the unit vector along the i-axis. In accordance with Ref. [29], by setting $v_1 = \theta$, $v_2 = z$, and $v_3 = r$, the corresponding metric coefficients are $h_1 = r$, $h_2 = h_3 = 1$. Thus, the nonzero components of the

surface displacement gradient tensor $\mathrm{grad}_S\mathbf{u}$ are

$$\begin{aligned}
(\mathrm{grad}_S\mathbf{u})_{11} &= (\mathrm{grad}\mathbf{u})_{11} = \frac{1}{r}\left(\frac{\partial u_\theta}{\partial\theta} + u_r\right), \quad (\mathrm{grad}_S\mathbf{u})_{12} = (\mathrm{grad}\mathbf{u})_{12} = \frac{\partial u_\theta}{\partial z},\\
(\mathrm{grad}_S\mathbf{u})_{21} &= (\mathrm{grad}\mathbf{u})_{21} = \frac{1}{r}\frac{\partial u_z}{\partial\theta}, \quad (\mathrm{grad}_S\mathbf{u})_{22} = (\mathrm{grad}\mathbf{u})_{22} = \frac{\partial u_z}{\partial z},\\
(\mathrm{grad}_S\mathbf{u})_{31} &= (\mathrm{grad}\mathbf{u})_{31} = \frac{1}{r}\left(\frac{\partial u_r}{\partial\theta} - u_\theta\right), \quad (\mathrm{grad}_S\mathbf{u})_{32} = (\mathrm{grad}\mathbf{u})_{32} = \frac{\partial u_r}{\partial z}.
\end{aligned} \tag{A3}$$

The projection tensor onto the tangent space is

$$\mathbf{P} = \mathbf{I} - \mathbf{e}_r\mathbf{e}_r = \mathbf{e}_\theta\mathbf{e}_\theta + \mathbf{e}_z\mathbf{e}_z. \tag{A4}$$

The tangential derivative tensor $\mathbf{D}_S\mathbf{u}$ of the displacement vector is obtained as

$$\begin{aligned}
\mathbf{D}_S\mathbf{u} = \mathbf{P}(\mathrm{grad}_S\mathbf{u}) &= (\mathrm{grad}\mathbf{u})_{11}\mathbf{e}_\theta\mathbf{e}_\theta + (\mathrm{grad}\mathbf{u})_{21}\mathbf{e}_z\mathbf{e}_\theta\\
&+ (\mathrm{grad}\mathbf{u})_{12}\mathbf{e}_\theta\mathbf{e}_z + (\mathrm{grad}\mathbf{u})_{22}\mathbf{e}_z\mathbf{e}_z.
\end{aligned} \tag{A5}$$

Thus, the first one in Eq. (A1) gives the following components of the surface strain tensor:

$$\begin{aligned}
&E_{11} = \frac{1}{r}\left(\frac{\partial u_\theta}{\partial\theta} + u_r\right), \quad E_{12} = E_{21} = \frac{1}{2}\left(\frac{\partial u_z}{r\,\partial\theta} + \frac{\partial u_\theta}{\partial z}\right)\\
&E_{22} = \frac{\partial u_z}{\partial z}, \quad E_{13} = E_{31} = E_{23} = E_{32} = E_{33} = 0
\end{aligned} \tag{A6}$$

Upon substituting Eq. (A6) into Eq. (A1.2), we obtain the following surface stress components:

$$\begin{aligned}
&\Sigma_{11} = \tau_0 + \frac{\lambda_0 + 2\mu_0}{r}\left(\frac{\partial u_\theta}{\partial\theta} + u_r\right) + (\lambda_0 + \tau_0)\frac{\partial u_z}{\partial z}, \quad \Sigma_{12} = \frac{\mu_0 - \tau_0}{r}\frac{\partial u_z}{\partial\theta} + \mu_0\frac{\partial u_\theta}{\partial z},\\
&\Sigma_{21} = (\mu_0 - \tau_0)\frac{\partial u_\theta}{\partial z} + \frac{\mu_0}{r}\frac{\partial u_z}{\partial\theta}, \quad \Sigma_{22} = \tau_0 + (\lambda_0 + 2\mu_0)\frac{\partial u_z}{\partial z} + \frac{\lambda_0 + \tau_0}{r}\left(\frac{\partial u_\theta}{\partial\theta} + u_r\right),\\
&\Sigma_{31} = \frac{\tau_0}{r}\left(\frac{\partial u_r}{\partial\theta} - u_\theta\right), \quad \Sigma_{32} = \tau_0\frac{\partial u_r}{\partial z}, \quad \Sigma_{13} = \Sigma_{23} = \Sigma_{33} = 0.
\end{aligned} \tag{A7}$$

Finally, by making use of the formulas in the Appendix of Ref. [29], we obtain for a cylindrical surface

$$\begin{aligned}
&\left(\rho_0\frac{\partial^2}{\partial t^2} + \frac{\lambda_0 + 2\mu_0}{r_0^2} - \frac{\tau_0}{r_0^2}\frac{\partial^2}{\partial\theta^2} - \tau_0\frac{\partial^2}{\partial z^2}\right)u_r\\
&+ \frac{\lambda_0 + 2\mu_0 + \tau_0}{r_0^2}\frac{\partial u_\theta}{\partial\theta} + \frac{\lambda_0 + \tau_0}{r_0}\frac{\partial u_z}{\partial z} + \sigma_{rr} + \frac{\tau_0}{r_0} = 0,\\
&- \frac{\lambda_0 + 2\mu_0 + \tau_0}{r_0^2}\frac{\partial u_r}{\partial\theta} + \left(\rho_0\frac{\partial^2}{\partial t^2} - \frac{\lambda_0 + 2\mu_0}{r_0^2}\frac{\partial^2}{\partial\theta^2} - \mu_0\frac{\partial^2}{\partial z^2} + \frac{\tau_0}{r_0^2}\right)u_\theta\\
&- \frac{\lambda_0 + \mu_0}{r_0}\frac{\partial^2 u_z}{\partial\theta\partial z} + \sigma_{r\theta} = 0,\\
&- \frac{\lambda_0 + \tau_0}{r_0}\frac{\partial u_r}{\partial z} - \frac{\lambda_0 + \mu_0}{r_0}\frac{\partial^2 u_\theta}{\partial\theta\partial z} + \left[\rho_0\frac{\partial^2}{\partial t^2} - \frac{\mu_0}{r_0^2}\frac{\partial^2}{\partial\theta^2} - (\lambda_0 + 2\mu_0)\frac{\partial^2}{\partial z^2}\right]u_z\\
&+ \sigma_{rz} = 0
\end{aligned} \tag{A8}$$

where r_0 is the finite radius of the cylindrical surface.

Equation (A8) gives the governing equations of the GM theory for an isotropic elastic material surface in the cylindrical coordinate system. It is clear that, when the surface tension vanishes, i.e., $\tau_0 = 0$, Eq. (A8) becomes identical to Eq. (19) in the text.

Appendix 2: Dispersion relation corresponding to the present first-order surface elasticity and the cutoff frequencies

If we retain the thickness effect in Eq. (11), then we obtain the dispersion relation governing the axisymmetric torsionless waves in a cylinder with surface effect as

$$g_{11}g_{22} - g_{12}g_{21} = 0 \tag{B1}$$

where

$$\begin{aligned} g_{1i} &= \left(-\rho^s h\omega^2 + \frac{a_1^s h}{r_0^2} - \frac{2c_{66}}{r_0}\right) J_1(\alpha_i r_0) + \left(c_{11}\alpha_i - c_{13}kp_i - \frac{a_2^s hk}{r_0}\right) p_i J_0(\alpha_i r_0) \\ &\quad + \delta h \left\{ \left[c_{44}k(k - \alpha_i p_i) - \frac{2c_{66}}{r_0^2}\left(\frac{c_{12}^s}{c_{11}^s} - 1\right)\right] J_1(\alpha_i r_0) \right. \\ &\quad \left. + \left[\frac{c_{11}\alpha_i - c_{13}kp_i}{r_0}\left(\frac{c_{12}^s}{c_{11}^s} - 1\right) - \frac{a_2^s k}{r_0} p_i \right] J_0(\alpha_i r_0) \right\}, \\ g_{2i} &= (-\rho^s\omega^2 + a_3^s k^2) p_i h J_0(\alpha_i r_0) + \left[c_{44}(k - \alpha_i p_i) - \frac{a_2^s hk}{r_0}\right] J_1(\alpha_i r_0) \\ &\quad + \delta h \left\{ \left[\frac{2c_{13}^s c_{66}k}{c_{11}^s r_0} - \frac{c_{44}}{r_0}(k - \alpha_i p_i)\right] J_1(\alpha_i r_0) - \frac{c_{13}^s k}{c_{11}^s}(c_{11}\alpha_i - c_{13}kp_i) J_0(\alpha_i r_0) \right\}. \end{aligned} \tag{B2}$$

For clarity, we have introduced a parameter δ such that $\delta = 1$ corresponds to the proposed surface elasticity with thickness effect, and $\delta = 0$ gives that without thickness effect, i.e., the GM surface elasticity theory.

For $k = 0$, the axial-shear motion is decoupled from the radial motion. The transcendental equation governing the cutoff frequencies for the axial-shear motion can be obtained as

$$(1 - \delta r_h) J_1(\Omega_s) = -r_\rho r_h \Omega_s J_0(\Omega_s), \tag{B3}$$

and that governing the cutoff frequencies for the radial motion is

$$\begin{aligned} &\left\{ \frac{a_1^s}{c_{44}} r_h - 2\frac{c_{66}}{c_{44}}\left[1 + \delta\left(\frac{c_{12}^s}{c_{11}^s} - 1\right) r_h\right] - r_\rho r_h \Omega_r^2 \right\} J_1(\Omega_r) \\ &= -\frac{c_{11}}{c_{44}}\left[1 + \delta\left(\frac{c_{12}^s}{c_{11}^s} - 1\right) r_h\right] \Omega_r J_0(\Omega_r) \end{aligned} \tag{B4}$$

where r_ρ and r_h are defined in Eq. (33), and

$$\Omega_s = r_0\omega\sqrt{\rho/c_{44}},\ \Omega_r = r_0\omega\sqrt{\rho/c_{11}}. \tag{B5}$$

When neglecting the thickness effect, Eqs. (B3) and (B4) become, respectively,

$$J_1(\Omega_s) = -r_\rho r_h \Omega_s J_0(\Omega_s), \tag{B6}$$

$$\left(\frac{a_1^s}{c_{44}} r_h - 2\frac{c_{66}}{c_{44}} - r_\rho r_h \Omega_r^2\right) J_1(\Omega_r) = -\frac{c_{11}}{c_{44}} \Omega_r J_0(\Omega_r). \tag{B7}$$

In view of Eq. (17), we can find that Eq. (B7) is the same as Eq. (10) in Ref. [37] when the material is isotropic. However, Eq. (B6) differs from Eq. (11) in Ref. [37] by a minus sign. We note that, when the surface effect is discarded, Eqs. (B6) and (B7) degenerate identically into the classical ones [48].

References

1. Kis, A., Mihailovic, D., Remskar, M., Mrzel, A., Jesih, A., Piwonski, I., Kulik, A.J., Benoît, W., Forró, L.: Shear and Young's moduli of MoS_2 nanotube ropes. Adv. Mater. **15**, 733–736 (2003)
2. Li, M., Tang, H.X., Roukes, M.L.: Ultra-sensitive NEMS-based cantilevers for sensing, scanned probe and very high-frequency applications. Nat. Nanotechnol. **2**, 114–120 (2007)
3. Lieber, C.M., Wang, Z.L.: Functional nanowires. MRS Bull. **32**, 99–104 (2007)
4. Gao, R.P., Wang, Z.L., Bai, Z.G., de Heer, W.A., Dai, L.M., Gao, M.: Nanomechanics of individual carbon nanotubes from pyrolytically grown arrays. Phys. Rev. Lett. **85**, 622–625 (2000)
5. Cuenot, S., Fretigny, C., Demoustier, C.S., Nysten, B.: Surface tension effect on the mechanical properties of nanomaterials measured by atomic force microscopy. Phys. Rev. B. **69**, 165410 (2004)
6. Chen, C.Q., Shi, Y., Zhang, Y.S., Zhu, J., Yan, Y.J.: Size dependence of Young's modulus in ZnO nanowires. Phys. Rev. Lett. **96**, 075505 (2006)
7. Shenoy, V.B.: Atomistic calculations of elastic properties of metallic fcc crystal surfaces. Phys. Rev. B. **71**, 094104 (2005)
8. Cao, G.X., Chen, X.: Size dependence and orientation dependence of elastic properties of ZnO nanofilms. Int. J. Solids Struct. **45**, 1730–1753 (2008)
9. Wang, J., Lu, C.S., Wang, Q., Xiao, P., Ke, F.J., Bai, Y.L., Shen, Y.G., Liao, X.Z., Gao, H.J.: Influence of microstructures on mechanical behaviours of SiC nanowires: a molecular dynamics study. Nanotechnology **23**, 025703 (2012)
10. Cammarata, R.C.: Surface and interface stress effects on interfacial and nanostructured materials. Mater. Sci. Eng. A **237**, 180–184 (1997)
11. Miller, R.E., Shenoy, V.B.: Size-dependent elastic properties of nanosized structural elements. Nanotechnology **11**, 139 (2000)
12. Dingreville, R., Qu, J.M., Cherkaoui, M.: Surface free energy and its effect on the elastic behavior of nano-sized particles, wires and films. J. Mech. Phys. Solids **53**, 1827–1854 (2005)
13. Gurtin, M.E., Murdoch, A.I.: A continuum theory of elastic material surfaces. Arch. Ration. Mech. Anal. **57**, 291–323 (1975)
14. Chen, T., Chiu, M.S., Weng, C.N.: Derivation of the generalized Young–Laplace equation of curved interfaces in nanoscaled solids. J. Appl. Phys. **100**, 074308 (2006)
15. Sharma, P., Ganti, S., Bhate, N.: Effect of surfaces on the size-dependent elastic state of nano-inhomogeneities. Appl. Phys. Lett. **82**, 535–537 (2003)
16. Wang, G.F., Feng, X.Q., Yu, S.W.: Surface buckling of a bending microbeam due to surface elasticity. Europhys. Lett. **77**, 44002 (2007)
17. Duan, H.L., Wang, J., Karihaloo, B.L.: Theory of elasticity at the nanoscale. Adv. Appl. Mech. **42**, 1–68 (2008)
18. Lu, P., He, L.H., Lee, H.P., Lu, C.: Thin plate theory including surface effects. Int. J. Solids Struct. **43**, 4631–4647 (2006)
19. Chen, W.Q., Zhang, Ch.: Anti-plane shear Green's functions for an isotropic elastic half-space. Int. J. Solids Struct. **47**, 1641–1650 (2010)
20. Lü, C.F., Wu, D.Z., Chen, W.Q.: Surface effects on the jump-in instability of nanomechanical structures. IEEE Trans. Nanotechnol. **10**, 962–967 (2011)
21. Liu, C., Rajapakse, R.K.N.D.: A size-dependent continuum model for nanoscale circular plates. IEEE Trans. Nanotechnol. **12**, 13–20 (2013)
22. Huang, Z.P., Wang, J.: A theory of hyperelasticity of multi-phase media with surface/interface energy effect. Acta Mech. **182**, 195–210 (2006)
23. Mindlin, R.D.: High frequency vibrations of plated, crystal plates. In: Progress in Applied Mechanics, pp. 73–84. MacMillan, New York (1963)
24. Gurtin, M.E., Murdoch, A.I.: Surface stress in solids. Int. J. Solids Struct. **14**, 431–440 (1978)
25. Tiersten, H.F.: Elastic surface waves guided by thin films. J. Appl. Phys. **40**, 770–789 (1969)
26. Rokhlin, S.I., Wang, Y.J.: Analysis of boundary conditions for elastic wave interaction with an interface between two solids. J. Acoust. Soc. Am. **89**, 503–515 (1991)
27. Bövik, P.: A comparison between the Tiersten model and O(h) boundary conditions for elastic surface waves guided by thin layers. J. Appl. Mech. **63**, 162–167 (1996)
28. Bövik, P.: On the modelling of thin interface layers in elastic and acoustic scattering problems. Q. J. Mech. Appl. Math. **47**, 17–42 (1994)
29. Benveniste, Y.: A general interface model for a three-dimensional curved thin anisotropic interphase between two anisotropic media. J. Mech. Phys. Solids. **54**, 708–734 (2006)
30. Ting, T.C.T.: Steady waves in an anisotropic elastic layer attached to a half-space or between two half-spaces—a generalization of love waves and Stoneley waves. Math. Mech. Solids. **14**, 52–71 (2009)
31. Chen, W.Q.: Surface effect on Bleustein–Gulyaev wave in a piezoelectric half-space. Theor. Appl. Mech. Lett. **1**, 041001 (2011)
32. Chen, W.Q.: Wave propagation in a piezoelectric plate with surface effect. In: Analysis of Piezoelectric Structures and Devices, pp. 285–312. Higher Education Press, Beijing (2013)
33. Wang, L.F., Hu, H.Y.: Flexural wave propagation in single-walled carbon nanotubes. Phys. Rev. B **71**, 195412 (2005)
34. Wu, X.F., Dzenis, Y.A.: Wave propagation in nanofibers. J. Appl. Phys. **100**, 124318 (2006)
35. Song, F., Huang, G.L., Varadan, V.K.: Study of wave propagation in nanowires with surface effects by using a high-order continuum theory. Acta Mech. **209**, 129–139 (2010)
36. Assadi, A., Farshi, B.: Size-dependent longitudinal and transverse wave propagation in embedded nanotubes with consideration of surface effects. Acta Mech. **222**, 27–39 (2011)
37. Huang, G.Y., Kang, Y.L.: Acoustic vibrations of a circular nanowire by considering the effect of surface. J. Appl. Phys. **110**, 023526 (2011)
38. Ding, H.J., Chen, W.Q., Zhang, L.C.: Elasticity of Transversely Isotropic Materials. Springer, Dordrecht (2006)
39. Timoshenko, S.P., Goodier, J.N.: Theory of Elasticity, 3rd edn. McGraw-Hill, New York (1970)

40. Chen, W.Q., Ding, H.J.: The state-space method and its application in analyses of FGM structures. In: Mechanics of Functionally Graded Materials and Structures, pp. 139–178. Nova Science Publishers, New York (2012)
41. Tarn, J.Q.: A state space formalism for anisotropic elasticity. Part II: cylindrical anisotropy. Int. J. Solids Struct. **39**, 5157–5172 (2002)
42. Ding, H.J., Chen, W.Q.: Three Dimensional Problems of Piezoelasticity. Nova Science Publishers, New York (2001)
43. Lur'e, A.I.: Three-Dimensional Problems of the Theory of Elasticity. Interscience Publishers, New York (1964)
44. Mindlin, R.D., McNiven, H.D.: Axially symmetric waves in elastic rods. J. Appl. Mech. **27**, 145–151 (1960)
45. Zhang, C.L., Liu, N., Yang, J.S., Chen, W.Q.: Thickness-shear vibration of AT-cut quartz plates carrying finite-size particles with rotational degree of freedom and rotatory inertia. IEEE Trans. Ultrason. Ferroelectr. Freq. Control **58**, 666–670 (2011)
46. Hirth, J.P., Lothe, J.: Theory of Dislocations, 2nd edn. Wiley, New York (1982)
47. Wang, G.F., Li, X.D.: Predicting Young's modulus of nanowires from first-principles calculations on their surface and bulk materials. J. Appl. Phys. **104**, 113517 (2008)
48. Mcniven, H.D., Mengi, Y.: Dispersion of waves in transversely isotropic rods. J. Acoust. Soc. Am. **49**, 229–236 (1971)
49. Hu, Y.G., Liew, K.M., Wang, Q., He, X.Q., Yakobson, B.I.: Nonlocal shell model for elastic wave propagation in single- and double-walled carbon nanotubes. J. Mech. Phys. Solids **56**, 3475–3485 (2008)
50. Wang, Q.: Wave propagation in carbon nanotubes via nonlocal continuum mechanics. J. Appl. Phys. **98**, 124301 (2005)
51. Hu, Y.G., Liew, K.M., Wang, Q.: Nonlocal elastic beam models for flexural wave propagation in double-walled carbon nanotubes. J. Appl. Phys. **106**, 044301 (2009)
52. Wang, Q., Liew, K.M.: Application of nonlocal continuum mechanics to static analysis of micro- and nano-structures. Phys. Lett. A **363**, 236–242 (2007)